Study on Uplift Bearing Characteristics of Micropiles in Weathered Rock With Shallow Overburden

Bing Feng[1], Weiming Ma[2], Yong Cai[3], Panfeng Li[1], Qi Zhang[2], Qing Lü[2*]

[1]Shaoxing Daming Electric Power Desin Institute, Shaoxing 312000, China
[2]College of Civil Engineering and Architecture, Zhejiang University, Hangzhou 310058, China
[3]Zhejiang Elecrtic Power Coproration of State Grid, Hangzhou 310008, China

*Corresponding author's e-mail: lvqing@zju.edu.cn

Abstract. In order to investigate the uplift bearing characteristics of micropiles in typical weathered rock with shallow overburden in mountainous areas of Zhejiang Province, China, the vertical uplift static load tests of micropiles were conducted in Ningbo, Taizhou, and Lishui by the Infrastructure Department of State Grid Zhejiang Corporation, respectively. This paper presented the Q-s curves, the axial force distribution of pile shafts, and the exertion of pile side friction of the micropiles obtained from these tests. Comparative analysis was made with the value of ultimate uplift bearing capacity calculated using the standard, and the modified calculated parameter was proposed. The results indicated that the Q-s curves of micropiles in weathered rock with shallow overburden appeared "steeply varying type", and the exertion of pile side friction was a dynamic process, which was related to factors such as geological properties, load grading, and tensile strength of pile materials. The main reason for the values of ultimate uplift bearing capacity calculated based on the standard being smaller than that measured was the smaller value of the uplift coefficient, and it was recommended that the value of the uplift coefficient in weathered rock with shallow overburden can be in the range of 0.85-0.94. The research findings provide a reference for the design and application of micropile foundations for transmission lines.

Keywords: weathered rock with shallow overburden; micropile; filed experiment; ultimate uplift bearing capacity; pile shaft friction; uplift coefficient

1 Introduction

The corridors of transmission lines in mountainous areas are tight, and a large number of transmission towers need to be built in high mountains or hilly areas.[1] They often encounter weathered rock foundations with shallow overburden. At present, the transmission tower in this kind of foundation often adopts rock embedded foundation, which has the advantages of high bearing capacity, small deformation and less backfilling. However, it has high requirements for geological conditions in application, such as shallow bedrock cover, construction should reduce the disturbance to rock mass, and construction space should be guaranteed. In contrast, the micro-pile foundation can be

W. Nie et al. (eds.), *Proceedings of the 2024 6th International Conference on Hydraulic, Civil and Construction Engineering (HCCE 2024)*, Atlantis Highlights in Engineering 37,
https://doi.org/10.2991/978-94-6463-726-7_18

constructed by mechanization, which has the technical advantages of fast construction, flexible layout, miniaturization of construction equipment, less site occupation and strong stratum adaptability, and has been applied more and more[2-3].

Micro-piles generally refer to bored piles with pile diameter not greater than 400 mm, which are used as the foundation of overhead transmission lines, and their design is mainly controlled by the uplift stability, and the key is to calculate the foundation's uplift bearing capacity. Some scholars have carried out research on the pullout bearing characteristics of micropiles, such as Sheng Mingqiang et al[4] carried out a comparative test on the pullout resistance of micropiles in loess site under water saturated and natural moisture content, the results show that the load-displacement curves under the water saturated condition are 'steeply varying', while under the natural condition, it is a three-stage 'slowly varying'. Tejinder et al[5] studied the effects of embedment ratio, diameter, relative density of soil and grouting pressure on the pullout capacity of micropiles in sandy soils using Taguchi method, which showed that the embedment ratio and diameter have the greatest influence on the pullout performance of micropiles, and the use of pressure grouting can control the deformation of micropiles. The deformation of micropiles can be controlled by pressure grouting. Xia Jun et al[6] established a finite element model of three- dimensional pile-soil interaction in soft ground based on the in-situ static load test of micropiles, and the calculation showed that the slope of the damage curve of the micropile foundation was greater after immersion, and the influence of the pile length on the ultimate bearing capacity of resistance to pullout and compression was more significant than that of the pile diameter.Hong et al[7] predicted the pullout bearing capacity of the micropile embedded in the soil based on the damage plane of soil around the micropile using an analytical method. The effects of the embedded length, diameter and surface roughness of the micropiles as well as the shear strength parameters of the soil were investigated. Based on the results of in-situ static load test, numerical simulation and theoretical analysis of micropiles in loess area, Kong Yang et al.[8] obtained the load bearing mode above and below the damage surface of the micropile, and put forward the prediction formula of ultimate resistance to pullout bearing capacity.

Although research has explored the pull-out performance of micro piles in different geological formations, there is still insufficient research on the shallow overburden weathered rock formations unique to mountainous areas. This study aims to fill this gap by conducting on-site experiments to analyze the tensile bearing characteristics of micro piles in such formations. In order to study the anti pull bearing characteristics of micro piles in typical shallow weathered rocks in mountainous areas, this study conducted vertical anti pull static load tests on micro piles in Ningbo, Taizhou, and Lishui. This article introduces the Q-s curves of micro piles obtained from three experiments, the distribution of axial force on the pile body, and the performance of pile side frictional resistance. Through comparative analysis with the ultimate bearing capacity calculated by the specifications, the revised calculation parameter values are proposed, providing reference for the design and promotion of micro pile foundations for transmission lines.

2 Overview of the Field Test Site

The field test was carried out in Ningbo, Taizhou and Lishui, Zhejiang. Test site one relies on the Tiechang-Xixi 110kV line project and is located near tower 69# in the northern part of Xidian Town, Ningbo, Ninghai County. Test site two relies on the Teshan-Xudu 110kV line project, located near the J12 corner tower in the northern part of Qinggang Town, Yuhuan City, Taizhou. Test site three relies on the Lixi-Muyun Π into Yunzhong Transformer 220kV line project, located in Lishui Yunhe County, Chongtou Town, Chongtou Town, near the village of the rock under the A8# tower position. The photos of each test site are shown in Fig. 1. According to the geological exploration report, all three sites are hilly terrain, and none of the boreholes revealed bedrock fissure water, and the stratigraphic parameters are shown in Table 1.

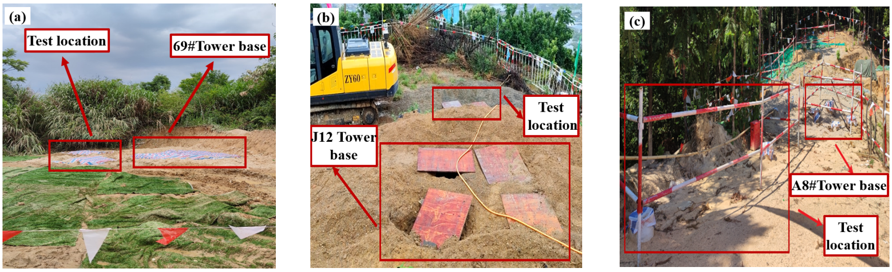

Fig. 1. Overview of the testing sites

Table 1. Stratigraphic parameters of the testing sites

Test point	Stratigraphic name	Layer thickness h/m	Unit weight γ/(kN/m^3)	Modulus of elasticity E_s/MPa	Poisson's ratio v_s	Cohesion c/kPa	Angle of internal friction φ/°	Limit side resistance standard value q_{sik}/kPa
Ningbo	Stockpile soil	1.0	18.0	20	0.32	15	13	50
	Fully weathered granite	10.2	19.3	700	0.45	33	23	70
Taizhou	Pulverised clay mixed with gravel	0.2	19.0	40	0.29	17	20	70
	Fully weathered tuff	1.5	20.0	600	0.40	32	25	120
	Strongly weathered tuff	6.3	22.5	1000	0.35	180	30	180
Lishui	Angular gravelly silty clay	0.9	17.0	50	0.28	14	21	68
	Fully weathered granite	7.3	18.0	600	0.38	12	25	110

3 Field Test Programme

3.1 Test Pile Design

A total of six monopiles were tested for vertical uplift static load at the three test sites, two at each site. The design dimensions of the test piles were the same, and the piles were all formed by C30 fine-grained concrete direct filling method, and the pile dimensions and reinforcement are shown in Table 2.

Table 2. Design parameters of the micropiles

Test site	Pile number	Diameter of pile /m	Pile length /m	Main reinforcement	Hoop reinforcement
Ningbo	P1	0.40	6.00	8ϕ18	1ϕ8+7ϕ14
	P2	0.40	6.00	8ϕ18	1ϕ8+7ϕ14
Taizhou	P3	0.40	6.00	10ϕ22	1ϕ8+6ϕ14
	P4	0.40	6.00	10ϕ22	1ϕ8+6ϕ14
Lishui	P5	0.40	6.00	8ϕ20	1ϕ8+7ϕ14
	P6	0.40	6.00	8ϕ20	1ϕ8+7ϕ14

Note: All steel bars used in the test piles are of HRB 400 grade.

3.2 Test Loading System

Before the test, the site was levelled, a concrete bedding was poured on the foundation and a steel mat was laid to provide support for the loading device. The uplift load was applied by a hydraulic centre-piercing jack with a range of 2000kN, which was placed on the steel beam, and the load was transferred to the main reinforcement of the pile body through the conversion fixture by counter-pressing the upper steel cover plate and tensioning the uplift screw, and the uplift load was controlled by the calibrated pressure gauge and pressure transducer. The schematic diagram of the test setup and the site photo are shown in Fig. 2.

3.3 Test and Measurement Systems

The displacement of the top of the pile under various levels of uplift loads was measured by means of a per centimeter meter. The dial gauge with a range of 50 mm and an accuracy of 0.01 mm was arranged symmetrically at the two ends of the pile head, and the gauge base was adsorbed on the reference beam. The vibrating string bar gauge was used to measure the axial force of the reinforcement at all levels of loading, and the bar gauge was welded to the four fixed sections of the main reinforcement of the pile body, and the arrangement was shown in Fig. 3. The principle of the rebar gauge to measure the rebar axial force Pij is shown in the following equation:

$$P_{ij} = K(f_{ij}^2 - f_{0j}^2) + B \tag{1}$$

In the formula, the subscripts i and j represent the loading level and section number, respectively; K and B are the calibration coefficients of the reinforcement gauge; f_{0j} is the frequency reading of the reinforcement gauge at the jth measured section before loading, and f_{ij} is the frequency reading of the reinforcing bar at the jth measured section under the ith level loading. The yield strain of reinforcement is much larger than the cracking strain of concrete, and the deformation of reinforcement can be regarded as linear elasticity before cracking of pile concrete, and the modulus of elasticity remains unchanged.

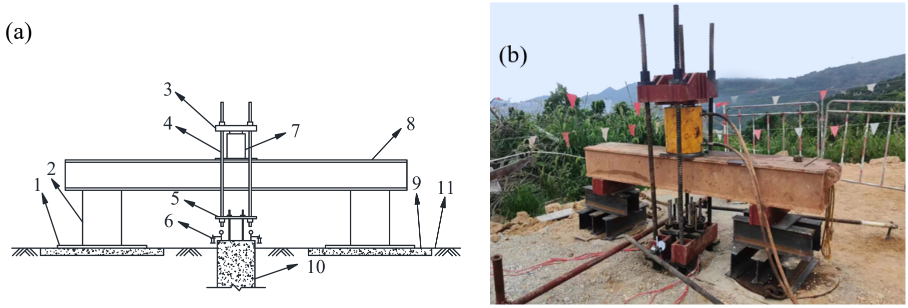

1—steel plate; 2—steel shim; 3—steel cover plate; 4—upward-drawing screw; 5—conversion Fixture; 6—reference beam; 7—hydraulic jack; 8—steel demand; 9—concrete bedding; 10—miniature pile; 11—ground level

Fig. 2. In-situ testing instruments

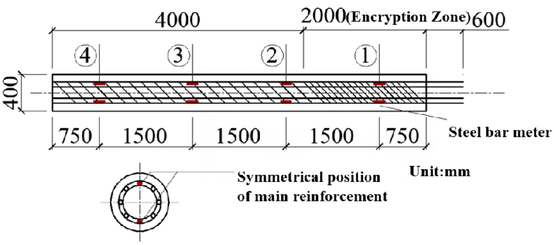

Fig. 3. Distribution of steel stress meters in piles

Assuming that the strains at the same cross-section of the pile body are equal everywhere, the strain of reinforcement obtained from the calculation of the axial force of the reinforcement can be taken as the strain of the concrete at that cross-section. It is generally believed that the deformation modulus of concrete is a constant, in the case of no consideration of cross-section change, the axial force of the pile body can be found by simple superposition of the axial force of the concrete and the axial force of the reinforcement obtained from the calculation of the concrete strain. Analysis shows that this calculation method will lead to a large calculation result of the pile body axial force, for which a correction using a non-linear model is required, which is discussed in Section 3.2 of this paper.

3.4 Field Test Process

After the piles were formed and cured for 28d, three standard concrete specimens with side length of 150mm were made at each site and tested to obtain the average values of compressive strength of 33.8 MPa, 32.2 MPa and 34.7 MPa respectively, which met the design requirements.

Before the test, the survival rate of the reinforcement gauge was checked by frequency meter. Due to improper operation of welding, pouring and maintenance, one reinforcement gauge failed at sections 2 and 4 of pile P1, sections 2 and 3 of pile P2, and sections 3 and 4 of pile P3 respectively. Since the failed reinforcement gauges were all at different sections, strain data were still available at all four sections of the pile body for each pile.

The destructive tests were carried out on all the micro-piles at the three sites. After the loading set-up was completed, preloading was carried out to ensure that the instrumentation was working properly. The loading was then carried out using the slow sustaining load method, with the reading time, stabilisation criteria, termination test conditions and the vertical ultimate bearing capacity against pullout determined in accordance with the specification.

4 Analysis of Test Results

4.1 Pile Load and Displacement Analysis

Figure 4 shows the relationship curves of single pile uplift load Q and pile top displacement s obtained from the field tests at each site. Taking the representative piles P2, P4 and P6 of the three sites, their Q-s curves are all of 'steep change type', and the load values corresponding to the starting point of the steep drop are taken as the vertical ultimate bearing capacity of the uplift, and the ultimate bearing capacities of the piles P2, P4 and P6 are 480 kN, 1210 kN and 700 kN respectively, which show good performance of the uplift bearing capacity. showed good performance of pullout load bearing.

According to the method recommended by the specification for pile foundation , combined with the stratigraphic parameters (Table 1), the pullout ultimate bearing capacity of the three test piles was calculated. The coefficient of resistance to pullout is determined according to the geological investigation report and the recommended value of the specification, which is taken as 0.5 for plain fill, 0.7 for gravelly chalky clay layer, 0.7 for fully-weathered rock layer, and 0.8 for strongly-weathered rock layer.The calculated pullout ultimate bearing capacity of P2, P4 and P6 piles are 339.3 kN, 948.8 kN and 547.3 kN, and the ratio to the test value is 0.71, 0.78 and 0.78, respectively, 0.78 and 0.78 respectively, indicating that the measured values of the three test piles are larger than the theoretical calculated values. There are two main reasons: (1) the standard value of ultimate lateral resistance of the ground is small; (2) the value of pullout coefficient is small.

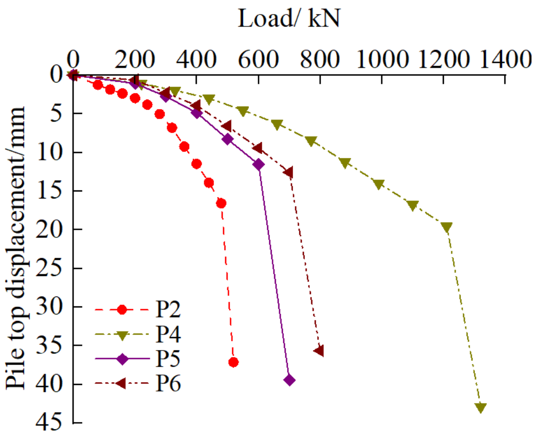

Fig. 4. Q-s curves of pull-out test for tested piles

4.2 Pile Axial Force Analysis

Generally, when calculating the axial force of the pile body, assuming the coordinated deformation of reinforcement and concrete, the following relationship is satisfied between the axial force of reinforcement Pij and the axial force of the pile body Nij, which is calculated according to equation (2):

$$N_{ij} = P_{ij} + \frac{P_{ij}}{A_{\mathrm{b}}}\left(A_{\mathrm{c}} - A_{\mathrm{b}}\right)\frac{E_{\mathrm{c}}}{E_{\mathrm{b}}} \tag{2}$$

Where: subscripts i and j represent the loading level and section number, respectively; *Nij* represents the axial force of the pile body at the jth measured section under the load of level i; A_c and A_b represent the cross-sectional area of the pile body and the total cross-sectional area of the main steel reinforcement, respectively; E_c and E_b represent the modulus of elasticity of the concrete and the steel reinforcement, respectively, and E_b is taken as 200 GPa.

Before pile cracking, the modulus of elasticity E_b of steel reinforcement can be considered to remain constant, while the tensile stress-strain relationship of concrete is more complicated and cannot be described by a simple linear elasticity model. The concrete material has poor tensile properties, and the microcracks produced by tension develop with the increase of uplift load, resulting in a gradual decrease in the modulus of the pile body and an increase in the tensile force borne by the steel reinforcement, and the results of the calculation of the pile body axial force obtained by using Eq. (2) are obviously large. Therefore, this paper adopts the concrete tensile stress-strain relationship model proposed by Zhenhai Jiao to consider the change of tensile modulus, and the relationship curve is shown below:

$$\begin{cases} y=\dfrac{\sigma_{\mathrm{t}}}{f_{\mathrm{t}}}=1.2x-0.2x^{6}, & 0\le x=\dfrac{\varepsilon_{\mathrm{t}}}{\varepsilon_{\mathrm{t0}}}\le 1 \\ y=\dfrac{\sigma_{\mathrm{t}}}{f_{\mathrm{t}}}=\dfrac{x}{\alpha_{\mathrm{t}}\left(x-1\right)^{1.7}+x}, & x=\dfrac{\varepsilon_{\mathrm{t}}}{\varepsilon_{\mathrm{t0}}}\ge 1 \end{cases} \tag{3}$$

Where: σ_t and ε_t are the concrete tensile stress and tensile strain; f_t is the uniaxial tensile strength of concrete; α_t is the parameter of the descending section of the curve; ε_{t0} is the peak tensile strain of concrete corresponding to f_t. Before pile cracking, it is considered that the reinforcement and concrete are deformed in a coordinated manner, and the stresses of reinforcement and concrete at the same strain are superimposed to obtain the stress-strain relationship of the pile and the axial force value of each measured section.

In fact, concrete reaches ultimate tensile strain before cracking. In this paper, it is assumed that the peak tensile strain of concrete is equal to the ultimate tensile strain, and 90×10^{-6} is taken as the peak tensile strain of C30 concrete of the pile body, and the concrete stresses that are in the descending section of the stress-strain curve after cracking are not calculated. The values of reinforcement tensile strain measured in the test exceeded the theoretically calculated values in many places, indicating that the pile showed different degrees of cracking in the process of uplift.

It can be seen from Fig. 5 that the average axial force of each measured section of the pile body generally shows an increase with the increase of uplift load and a decrease with the increase of depth, and there are differences in the rate of decrease in different strata, which reflects a process of top-down transfer of the internal force of the micropile. The three piles still have a certain size of axial force near the bottom of the pile end (-5.25m), which should be the sum of lateral frictional resistance of the pile body below the bottom of the pile end and the suction force at the bottom of the pile caused by upward pulling action. It is believed that the bearing capacity of the pile is mainly provided by the pile side frictional resistance and the pile weight, and the bottom suction force is small and difficult to measure, which can be ignored in general. In this paper, it is assumed that the axial force at the bottom of the pile is zero.

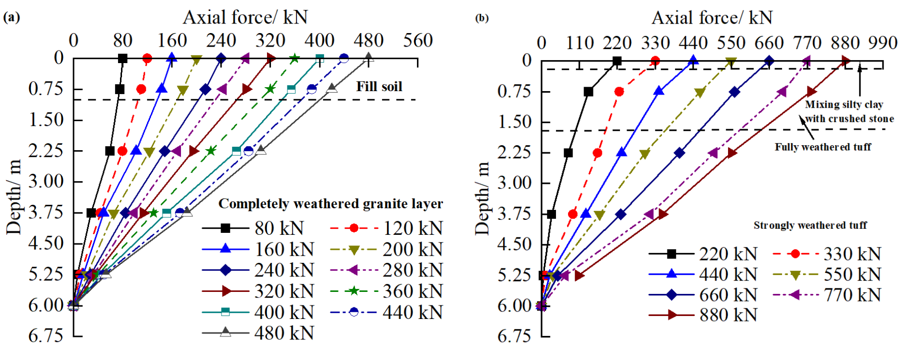

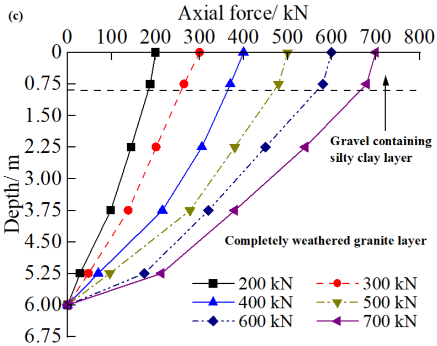

Fig. 5. Distribution of pile shaft axial force

The axial force distribution curve of the pile body can reflect the pullout resistance provided by the soil on the pile side, and the axial force distribution curve of each pile changed with the loading. For P2 pile, the axial force of the pile body was basically linearly distributed, and the slope of the distribution straight line gradually decreased with the increase of loading, which indicated that the pile-side friction force was gradually exerted from top to bottom. During the whole loading process, the slope of the straight line of axial force distribution in the lower part of the pile (below -2.25 m) was always smaller than that in the upper part (above -0.75 m), reflecting that the lateral friction resistance of the lower fully weathered granite layer was greater than that of the upper plain fill layer. After loading to 400 kN, the linear slope of the lowest pile section (-3.75 m~-5.25 m) basically remains unchanged, indicating that the lateral friction resistance of the corresponding pile section is fully exerted.

4.3 Analysis of Pile Lateral Frictional Resistance

The top of the pile is noted as the measurement section No. 0, the cross sections of the arrangement of the reinforcement gauge are noted as sections No. 1 to No. 4 from top to bottom, and the portion of the pile body between the measurement sections No. j-1 and No. j is noted as the section of the pile No. j. Assuming that the pile-side mechanical resistance is evenly distributed between the two measured sections, the pile-side mechanical resistance fsi,j of pile section No. j under the load of level i can be calculated by the following formula:

$$f_{\mathrm{s}i,j} = \frac{N_{i,j-1} - N_{i,j} - W_j}{U_{\mathrm{p}} h_j} \tag{4}$$

Where: $N_{i,j-1}$ and $N_{i,j}$ are the axial forces of the pile body at the j-1st and jth measured sections, respectively; W_j is the deadweight of the jth pile section; U_p is the perimeter of the pile section; and h_j is the height of the jth pile section.

Figure 6 demonstrates the distribution of pile lateral friction force with depth for each pile (the boxed data points correspond to the cracked area of the pile body above the depth). From the figure, it can be seen that the uplift load carried by the pile is transferred to the surrounding strata in the form of shear force.

For P2 pile, in the early loading stage, due to the short pile body and the weak vertical friction constraint on the pile body by the soil fill layer, the uplift load is mainly borne by the lateral friction resistance of the lower fully weathered granite layer. With the increase of uplift load, the lateral friction resistance of each stratum was gradually exerted, and finally the lateral friction resistance of the pile in the fully weathered granite layer tended to stabilise when approaching the ultimate load, and reached a maximum of 60~70 kPa.

Before the uplift load of P4 pile reaches 550 kN, the lateral friction resistance is roughly distributed in the form of a step-like distribution with the upper soil-rock composite layer being larger and the lower strongly weathered rock layer being smaller, and the lateral friction resistance of the pile in the lower strata mainly contributes to the resistance to uplift bearing capacity only after 550 kN. The reason is that, on the one hand, the reinforcement stress gauges are set at the fixed section of the pile body, which cannot reflect the distribution of the pile lateral resistance in the upper single stratum, and the pile lateral resistance of the upper composite stratum consisting of pulverised clay mixed with gravel layer and fully weathered tuff layer bears most of the uplift load in the early loading stage, and the latter has a greater contribution; on the other hand, the large loading grading in the test results in that the pile lateral resistance of the upper strata gives full play to the pile lateral resistance at the early loading stage, and then the pile lateral resistance increases as the pile load is applied to the lower strata with a greater contribution. On the other hand, the large load grading of the test resulted in the pile lateral resistance of the upper stratum being fully utilised at the early stage of loading, and then with the increase of load on the top of the pile, the cracking area expanded, and the maximum value of the pile lateral resistance gradually shifted to the lower part of the pile. Finally, the maximum pile-side resistance in the strongly weathered tuff layer reached 120~130 kPa.

At the early stage of loading, the distribution of pile-side mechanical resistance of pile P6 was similar to that of pile P2, with the depth distribution showing the characteristics of small upper breccia-bearing silty clay layer and large lower fully weathered granite layer. As loading proceeds, the distribution of pile-side mechanical resistance changes similarly to that of pile P4, i.e., due to the larger load classification, the pile-side mechanical resistance in the lower fully weathered granite layer increases significantly, while the pile concrete in the breccia-bearing chalky clay layer cracks earlier, and the pile-side mechanical resistance in the fully weathered granite layer eventually reaches a maximum of 105~115 kPa.

The analysis shows that the play of pile lateral friction resistance is a dynamic process, and its play is related to the nature of the stratum, load grading and the tensile strength of the pile body material and other factors. When the upper stratum is plain fill or gravelly silty clay with poor properties, the pile lateral mechanical resistance in the lower weathered rock layer will play a role at the beginning of loading, and the pile lateral mechanical resistance with the depth of burial shows the distribution of the upper stratum is small and the lower stratum is large. However, when the load rating of the test was larger or the upper stratum was a soil-rock composite stratum (e.g., P4 pile), the pile-side molecular resistance in the upper stratum was more fully utilised at the beginning of the loading period compared with that in the lower strongly weathered rock stratum, and the concrete in the pile body cracked due to the low tensile strength during the application of the first two or three loads. Afterwards, with the increase of load on the top of the pile, the cracked area was enlarged and the peak of pile-side molecular resistance gradually shifted to the lower part of the pile body.

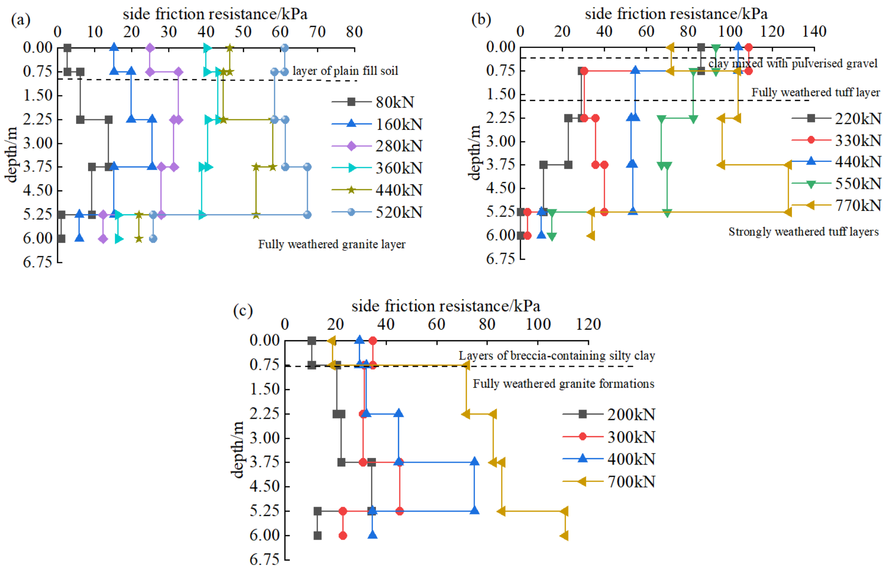

Fig. 6. Distribution of pile shaft friction

4.4 Analysis of Pile Bearing Performance

For layered foundations, a weighted average of lateral friction resistance with the thickness of layered soil and rock on the side of the pile as weights can be used as an overall calculation parameter, i.e.

$$f_s = \frac{\sum f_{si} H_i}{\sum H_i} \tag{5}$$

Where: f_{si} and H_i are the values of lateral molecular resistance of each stratum on the pile side and the thickness of the stratum, respectively.Table 3 lists the weighted average values of the measured maximum pile side mechanical resistance of the whole pile body and the weighted average values of the pile side mechanical resistance in the ground investigation report when P2, P4 and P6 piles reached the ultimate bearing capacity for elevation. It can be seen from the table that the measured values are smaller than the recommended values in the ground investigation report. Combined with the analyses in Section 3.1, it can be concluded that the main reason for the measured ultimate bearing capacity to resist pullout being larger than the theoretical calculated value is that the recommended pullout coefficient in the specification is small.

Table 3. Comparison between the weighted average value of the maximum measured pile shaft friction and the recommended values

pile number	Weighted value of measured maximum pile lateral resistance f_{s1}/kPa	Recommended Weighted Pile Side Frictional Resistance Values f_{s2}/kPa	f_{s1}/f_{s2}
P2	61.9	66.7	0.93
P4	114.7	161.3	0.71
P6	71.2	103.7	0.69

The existing experimental and numerical simulation studies show that the pile side friction resistance of the resistant pile is smaller than that of the compressive pile, i.e., the coefficient of resistance λ exists, and $\lambda \leq 1$. Some scholars carried out a relevant study on this difference, which is considered to be mainly caused by the Poisson's ratio effect, the change of the total stress field, and the rotation of the principal stress axis. The latter two are more difficult to study theoretically and are mainly studied by model tests or numerical simulations. In this paper, only the Poisson's ratio effect is considered to correct the coefficient of resistance to pullout. When the pile is subjected to axial load, due to the Poisson effect, the pile undergoes radial shrinkage, which affects the frictional force between the pile and the surrounding soil. This study considers this effect by adjusting the pull-out coefficient to reflect the influence of Poisson's ratio on pile side friction resistance.

When the pile is loaded, the Poisson effect causes radial contraction, resulting in a decrease in the normal stress on the pile side, which in turn reduces the friction between the pile and the ground, while the opposite is true for the compressive pile. Considering the difference in pile-side friction due to Poisson's ratio effect, there are:

(1) The sum of pile-side frictional resistance Qt for a pile with resistance to pile pullout:

$$Q_{\mathrm{t}} = [p_{\mathrm{b}}^{'} - \frac{D(1+BL)}{B^2}]e^{-BL} + \frac{D}{B^2} \tag{6}$$

(2) Sum of pile-side friction forces Qc for compressive piles (compressive piles are assumed to be complete friction piles):

$$Q_{\mathrm{c}} = [p_{\mathrm{b}} - \frac{D(1-BL)}{B^2}]e^{BL} + \frac{D}{B^2} \tag{7}$$

(3) Calculation of the coefficient of pullout resistance:

$$\lambda = \frac{Q_{\mathrm{t}}}{Q_{\mathrm{c}}} \tag{8}$$

In the above equation, $B=2\pi dGv_p tan\delta/AE_p$; $D=\pi dK_0\gamma tan\delta$; p_b' is the tension at the bottom of the pile section (take 0 at the bottom of the pile); p_b is the pressure at the bottom of the pile section (take 0 at the bottom of the pile); L is the layer thickness of the corresponding strata; d is the diameter of the pile; G is the shear modulus of the ground stratum around the pile, which is calculated according to $E_s/2(1 + v_s)$, Poisson's ratio of the pile; δ is the friction angle between pile and soil, calculated by 0.75φ, and φ is the internal friction angle of the strata; E_p is the elastic modulus of the pile; K_0 is the coefficient of static earth pressure, calculated by $1\text{-}sin\varphi$; and γ is the heaviness of the strata. Starting from the bottom of the pile upwards, the pile lateral frictional resistance in each stratum is calculated, and then the pullout coefficient of the corresponding stratum is calculated, and the specific calculation process of the pullout coefficient of each stratum is referred to the literature. The corrected pullout coefficients according to Eqs. (6), (7) and (8) and the ultimate pullout capacities calculated using the corrected pullout coefficients are shown in Table 4, from which it can be seen that the corrected pullout coefficients range from 0.85 to 0.94, and the ultimate pullout capacities calculated using the corrected pullout coefficients are closer to the field measured values. By comparing theoretical calculations with actual test results, we can verify the applicability of the theoretical model and adjust design parameters accordingly.

Table 4. Comparison between the modified calculated ultimate uplift bearing capacity and the calculated values based on standards

Pile number	Stratum (geology)	Modified pull-out coefficient	Measured Ultimate Elevation Capacity T_1/kN	Calculated value of ultimate pull-out capacity T_2/kN	Correction of the calculated value of the ultimate pull-out capacity T_3/kN	$\frac{\lvert T_1 - T_2 \rvert}{T_1}$	$\frac{\lvert T_1 - T_3 \rvert}{T_1}$
P1	Stockpile soil	0.937	480	339.3	470.5	0.29	0.02
	Fully weathered granite	0.936					
P4	Pulverised clay mixed with gravel	0.874	1210	948.8	1254.4	0.22	0.04
	Fully weathered tuff	0.874					
	Strongly weathered tuff	0.890					
P6	Angular gravelly silty clay	0.922	700	547.3	720.9	0.22	0.03

5 Conclusion

In order to study the pullout bearing characteristics of micropiles in weathered rock with typical shallow cover in mountainous areas of Zhejiang Province, the vertical pullout static load tests of micropiles were carried out in Ningbo, Taizhou and Lishui respectively. In this paper, the *Q*-*s* curves of the micro-piles, the axial force distribution of the pile body and the friction force on the pile side obtained from the three tests are presented, and the corrected values of the calculation parameters are proposed by comparing and analysing them with the ultimate bearing capacity obtained from the specification calculations. The following conclusions are mainly obtained:

(1) The uplift *Q*-*s* curve of micropiles in weathered rock with shallow cover is 'steeply variable';

(2) The tensile stress-strain relationship of pile concrete is nonlinear, and the concrete axial force calculated by the fixed modulus of elasticity is obviously large, while the concrete axial force calculated by the tensile stress-strain relationship model of concrete is more accurate;

(3) The exertion of pile lateral friction force is a dynamic process, and its exertion is related to factors such as the nature of the stratum, the grading of the load and the tensile strength of the pile body material;

(4) Comparative analysis of the field test results and the calculation results of the current specification shows that the small value of the coefficient of resistance to pullout is the main reason that the measured value of the ultimate bearing capacity of pullout is larger than the theoretical calculated value, and after the correction of the coefficient of resistance to pullout, the measured and theoretical calculated values are closer to each other, and the coefficient of resistance to pullout of the corrected strata is in the range of 0.85~0.94.

Although this study provides empirical data on the pull-out performance of micro piles in weathered rocks, there are some limitations in the research, such as limited sample size and failure to cover all possible geological variants. Future research can expand the sample size, further validate the findings of this study, and explore the long-term performance of micro piles under different geological conditions.

Acknowledgment

This work received financial support from the Shaoxing Jianyuan Power Group Co.,Ltd. Technology Project (CF058506002022001).

References

1. CUI Q, CHENG Y, LU X, et al. Study on pullout test and load-displacement curve model parameters of excavated foundation in strongly weathered rock. Geotechnics, 2018, 39(12): 4597-4604.
2. EDITORIAL BOARD OF CHINESE JOURNAL OF HIGHWAY. Review of academic research on roadbed engineering in China-2021. China Highway Journal, 2021, 34(3): 1-49.
3. ZHANG A, FU H, WANG J, et al. Study on the pullout bearing capacity of miniature group piles and the effect of group piles on loess foundations. Building Structure, 2022, 52(24): 120-125.

4. SHENG M, QIAN Z, YANG W, et al. Tests on compressive and pullout bearing capacity of loess micropiles under water-saturated conditions. Journal of Geotechnical Engineering, 2021, 43(12): 2258-2264.
5. TEJINDER T, VINAY C, VENKATA K. Multi-parameter experimental study on the factor contributions of micropile uplift capacity using Taguchi approach. International Journal of Geosynthetics and Ground Engineering, 2023, 9(4): [page range needed].
6. XIA J, BAI H, WANG J, et al. Study on uplift and downward bearing performance of micropile foundation in loess. Journal of Applied Mechanics, 2023, 40(2): 340-349.
7. HONG W, CHIM N. Prediction of uplift capacity of a micropile embedded in soil[J]. KSCE Journal of Civil Engineering, 2015, 19(1).
8. KONG Y, RUAN H, HUANG X, et al. Study on the action mechanism of micro-piles for pull-out anchorage of photovoltaic mounts. Journal of Solar Energy, 2020, 41(2): 262-267.